

OPEN ACCESS

EDITED BY Abel Ramoelo, University of Pretoria, South Africa

REVIEWED BY Leiku Yang, Henan Polytechnic University, China Xing Wang, University of Nanking, China

*CORRESPONDENCE Alexei Lyapustin, ☑ Alexei.i.lyapustin@nasa.gov

RECEIVED 31 July 2025 ACCEPTED 30 September 2025 PUBLISHED 20 October 2025

CITATION

Lyapustin A, Choi M, Wang Y, Korkin S, Hyer E and Marshak A (2025) Simultaneous retrieval of aerosol optical depth, spectral absorption and layer height from DSCOVR EPIC using MAIAC algorithm.

Front. Remote Sens. 6:1677438. doi: 10.3389/frsen.2025.1677438

COPYRIGHT

© 2025 Lyapustin, Choi, Wang, Korkin, Hyer and Marshak. This is an open-access article distributed under the terms of the Creative Commons Attribution License (CC BY). The use, distribution or reproduction in other forums is permitted, provided the original author(s) and the copyright owner(s) are credited and that the original publication in this journal is cited, in accordance with accepted academic practice. No use, distribution or reproduction is permitted which does not comply with these terms.

Simultaneous retrieval of aerosol optical depth, spectral absorption and layer height from DSCOVR EPIC using MAIAC algorithm

Alexei Lyapustin^{1*}, Myungje Choi², Yujie Wang², Sergey Korkin², Edward Hyer³ and Alexander Marshak¹

¹NASA Goddard Space Flight Center, Greenbelt, MD, United States, ²University of Maryland Baltimore County, Baltimore, MD, United States, ³Naval Research Laboratory, Monterey, CA, United States

A novel MAIAC algorithm is described for joint retrievals of the aerosol optical depth, spectral absorption and layer height (ALH) from DSCOVR EPIC observations in the UV-Vis-NIR spectral range including atmospheric oxygen A- and B-bands. While the oxygen bands have been used to estimate ALH in several existing algorithms, MAIAC for the first time employs a synergy between the UV and O₂ A,B-bands to enhance sensitivity to the height of aerosol layer and retrieves it simultaneously with other major aerosol properties. The ALH retrieval capability is illustrated using several examples for smoke and dust aerosols over different parts of the globe. A global AERONET validation of aerosol properties based on the full EPIC data record (mid-2015-2025) shows an accuracy of AOD with correlation coefficient R ~ 0.71-0.73, RMSE ~ 0.4, and expected error EE ~ 20%. While accuracy of AOD is moderate due to the backscattering view geometry of EPIC, achieved agreement of spectral single scattering albedo (SSA) at 443 and 680 nm with AERONET inversion data is very good: the expected error ± 0.03 agrees with AERONET uncertainty, the RMSE is within 0.02-0.03, and bias is within ± 0.01 . The ALH product was validated globally for the overlapping EPIC- CALIOP CALIPSO period using the CALIPSO total backscatter weighted height. The ALH validation shows a robust performance with global RMSE ~ 1.1 km and 60%-77% of retrievals within $EE = \pm 1$ km. The retrieved ALH is lower than CALIOP ALH_C by 0.45-0.75 km over land and is unbiased over the ocean. This new capability and suite of aerosol products, designed to support both the Earth system modeling and the air quality applications, are part of the version 3 MAIAC EPIC algorithm. The v3 algorithm has recently completed reprocessing of the EPIC record covering the period of 2015-2025.

KEYWORDS

EPIC, MAIAC, CALIOP, aerosol layer height, biomass burning, mineral dust, spectral absorption

1 Introduction

Widely varying properties of absorbing aerosols, generated by wildfires and dust storms, are a significant source of uncertainty in the Earth system models (Boucher et al., 2013). Satellite based information on loading, absorption, size distribution and vertical profile of atmospheric aerosols derived from active and passive sensors provides important constraints for regional to global chemical transport, aerosol forecast and climate

models. Aerosol properties and height also define the near-surface visibility and quality of the breathable air affecting both human and environmental health. Existing trends of the increasing intensity and frequency of wildfires in particular over North America raise significant public health concerns (Westerling et al., 2006; Wei et al., 2023) stipulating further developments in improving satellite-based monitoring of aerosol properties.

Global characterization of aerosol loading, or aerosol optical depth (AOD), has been the main satellite product from single-look passive on-orbit sensors such as MODIS, VIIRS, ABI, etc. (Levy et al., 2013; Lee et al., 2024; Kondragunta et al., 2020; Lyapustin et al., 2018). Torres et al. (1998), Torres et al. (2013), and Torres et al. (2020) additionally retrieves single scattering albedo (SSA) from sensors with UV channels (e.g., TOMS, OMI, TROPOMI), by using assumed values for spectral dependence of absorption, aerosol size distribution and aerosol layer height (ALH). Spectral dependence of absorption, or refractive index (k_{λ}) , carries information about aerosol chemical composition (e.g., Schuster et al., 2016; Li et al., 2019) and should be retrieved from satellite data. Coupled with AOD, k_{λ} can be used to infer volume and mass fractions of the main absorbers in the UV-vis spectrum, such as black and brown carbon in smoke (Choi et al., 2024) or hematite and goethite in airborne dust (Go et al., 2022). Aerosol composition, in turn, is an important input both to models and to epidemiology research establishing links between the health outcomes and speciated particulate matter (e.g., Diner et al., 2018).

Several approaches were developed to estimate ALH or AOD-ALH combination using measurements in atmospheric oxygen O₂ A- and B-bands from passive sensors (Sanders and de Haan, 2013; Nanda et al., 2020; Xu F. et al., 2017; Xu et al., 2019; Lu et al., 2021; Chen et al., 2021; de Graaf et al., 2025). Recent multi-angle polarimetric sensors such as POLDER, AirMSPI, DPC, POSP, HARP2, and SpexOne can enable the simultaneous retrieval of multiple aerosol properties, including particle size and complex refractive index, using their rich information content (Dubovik et al., 2011; Dubovik et al., 2019; Xu F. et al., 2017; Xu et al., 2019; Hasekamp et al., 2019; Li et al., 2019; Li et al., 2022; Chen et al., 2025; Martins et al., 2024; Fu et al., 2025).

Previously, we reported a novel approach using the Multi-Angle Implementation of Atmospheric Correction (MAIAC) algorithm for simultaneous retrieval of AOD and spectral aerosol absorption from the Earth Polychromatic Imaging Camera (EPIC) UV-Vis observations (Lyapustin et al., 2021b) onboard the NOAA's Deep Space Climate Observatory (DSCOVR). The MAIAC v2 algorithm uses assumed values for regional aerosol type (smoke or dust), size distribution, and aerosol layer height based on climatology. Although the assumed aerosol properties are generally representative, they can introduce biases in the retrieved properties, particularly under heavy plume conditions with large variability in aerosol characteristics. For example, different assumptions about smoke height (e.g., 1 km vs. 4 km) can lead to a difference in SSA of about 0.03, as both aerosol height and absorption influence the degree of multiple scattering of light (Lyapustin et al., 2021b). According to Sun et al. (2019), even with the same UV aerosol index, a bias in ALH can lead to an SSA bias of up to ~0.06. The same study also showed that assumptions about spectral absorption characteristics (e.g., spectrally flat vs. strongly wavelength-dependent) can result in SSA biases of up to \sim 0.25. This paper describes our further developments to address these limitations, most significantly the addition of simultaneous retrieval of ALH in the latest version 3 MAIAC EPIC algorithm with the use of the EPIC's oxygen absorption bands.

This paper is structured as follows: Section 2 gives an overview of the MAIAC EPIC algorithm, an overview of the previous v2 algorithm, and a detailed description of the latest v3 developments. Section 3 gives examples of ALH retrievals for different smoke and dust events. A global full-mission validation analysis of both aerosol optical properties and layer height is given in Section 4. This paper concludes with the Summary section.

2 MAIAC EPIC processing algorithm

The DSCOVR satellite is located at Lagrange-1 (L1) orbit approximately 1.5 million km from the Earth towards the Sun. It carries two Earth science instruments, one of them is EPIC with 10 narrowband channels (317, 325, 340, 388, 443, 551, 680, 688, 764 and 779 nm). Nadir horizontal resolution is 8 km in the Blue (443 nm) band; in all other bands, the resolution is 16 km due to the 2×2 pixel onboard aggregation introduced to reduce the data transmission rate. Due to DSCOVR's unique orbit, EPIC continuously observes the entire sunlit side of the Earth and provides 10-12 observations for the same surface area from dawn to dusk in summer, and 6-7 images in winter (Marshak, et al., 2018). This high temporal coverage, enabled by its orbit, provides a unique advantage for monitoring diurnal variations on a global scale using a single sensor. All observations are acquired near the backscattering direction, with scattering angle ranging between 168° and 178°.

2.1 Overview

The MAIAC EPIC algorithm consists of two parts including standard processing and advanced aerosol characterization. The standard MAIAC processing (Lyapustin et al., 2021a) performs cloud detection that is coupled with detection of absorbing aerosols, retrieval of AOD for cloud-free pixels using the background aerosol model, and an atmospheric correction providing spectral surface bidirectional reflectance factors (BRF) and bidirectional reflectance distribution function (BRDF) model. MAIAC algorithm uses scaled Ross-Thick Li-Sparse (sRTLS) BRDF model (Lyapustin et al., 2025). Compared to standard RTLS model (Wanner et al., 1995), sRTLS adds the Maignan et al. (2004) hot-spot factor to the volumetric kernel, which is important to EPIC given its near hot-spot view geometry, and corrects behavior at high zenith angles above 60°. The background aerosol models for AOD retrievals are defined for nine world regions based on climatology analysis of the version 3 AERONET inversion database (Holben et al., 1998; Giles et al., 2019). Using the dynamic time series analysis and the minimum reflectance method, MAIAC also derives the per-pixel spectral regression coefficients (SRC) required for aerosol retrievals. SRC represents spectral ratios of surface reflectance (ρ_{443}/ρ_{680} , $\rho_{388}/$ ρ_{680} , and ρ_{340}/ρ_{388}), where surface reflectance (SR) ρ is a result of Rayleigh and background aerosol atmospheric correction (Lyapustin et al., 2018; Lyapustin et al., 2021a).

The standard processing starts with gridding EPIC's geolocated and calibrated level 1B (L1B) data to 10 km resolution using Zonal Sinusoidal Projection (ZSP) described in Lyapustin et al. (2021a). ZSP minimizes spatial distortions typical to the global Sinusoidal projection. Gridding allows us to, effectively, "observe" the same grid cell over time at different Sun-view angles and perform surface characterization for each grid cell including spectral BRDF, NDVI and SRC. This information, stored for every grid cell, supports detection of clouds and absorbing aerosols, and helps retrievals of aerosol properties. Finally, it's worth mentioning that the MAIAC surface dataset is naturally gap-filled: data from the previous retrievals stay in operational memory for each grid cell until dynamically updated from the latest cloud-free observations. Such dynamic update helps MAIAC surface model to adapt to changing land surface conditions, driven by vegetation seasonality, rapid change etc., over time.

Given a reliable characterization of spectral surface reflectance by MAIAC, a well calibrated set of EPIC's visible (443 and 680 nm) and UV channels (340 and 388 nm) offers a unique opportunity to simultaneously retrieve both AOD and spectral absorption of aerosols.

2.2 MAIAC v2 algorithm: joint retrieval of AOD and spectral absorption

With the knowledge of surface reflectance, we can use the Blue and UV channels to retrieve both AOD and spectral aerosol absorption. As mentioned before, spectral dependence of absorption carries information on particles chemical composition, including black-brown carbon partitioning for smoke, or hematite/goethite content for the mineral dust. In this work, spectral absorption is represented by a conventional power-law expression (e.g., Bond, 2001; Kirchstetter et al., 2004), given by Equation 1:

$$k_{\lambda} = k_0 (\lambda/\lambda_0)^{-SAE}$$
 for $\lambda < \lambda_0$, and $k_{\lambda} = k_0$ for $\lambda \ge \lambda_0$, where λ_0
= 680 nm (1)

where k is an imaginary refractive index. In the limit of small (fine mode) particles, the spectral absorption exponent (SAE) is related to the conventional Absorption Angstrom Exponent (AAE) that defines spectral dependence of the aerosol absorption optical depth (AAOD) as $SAE \sim AAE$ -1 (Moosmüller and Chakrabarty, 2011).

We are using Levenberg-Marquardt optimal fit algorithm (Marquardt, 1963) to derive the unknowns (AOD_{443} , k_0 , SAE) by matching EPIC TOA reflectance at 340, 388, 443 nm:

$$F^{2} = \frac{1}{N} \sum \left[\frac{L_{\lambda}^{m} - L_{\lambda}^{t}}{L_{\lambda}^{m}} \right]^{2} = min\{AOD_{443}, k_{0}, SAE\},$$
 (2)

where L_{λ}^{m} and L_{λ}^{t} are measured and theoretical, or simulated, values, respectively. The retrievals are based on the look-up table (LUT) computed with combination of vector code IPOL (Korkin and Lyapustin, 2023) providing path reflectance and scalar code SHARM (Lyapustin, 2003; Lyapustin, 2005) generating atmospheric Green's function, transmittance, and spherical albedo.

The real refractive index (m) and size distribution for both smoke and dust models are fixed. Specifically, the smoke model uses m=1.48 and a bimodal lognormal size distribution with $r_{\rm vf}=0.14$, $\sigma_{\rm vf}=0.4$, $r_{\rm vc}=2.8$, $\sigma_{\rm vc}=0.6$, $C_{\rm vf}/C_{\rm vc}=2.5$. Here, $r_{\rm v}$, $\sigma_{\rm v}$ are the volumetric radius and standard deviation, and $C_{\rm v}$ is the volumetric concentration for the fine (f) and coarse (c) modes, respectively. The dust LUT uses model of randomly oriented spheroids (Dubovik et al., 2006) with m=1.56, following the dynamic model of Dubovik et al. (2002) for the Solar Village site in Saudi Arabia where the relative concentration of the coarse mode dust grows rapidly with AOD.

The LUTs are generated on a 4×4 matrix of $SAE = \{0.1, 1.5, 3, 4\}$ and $k_0 = \{0.001, 0.006, 0.011, 0.016\}$ for smoke and $k_0 = \{0.0006, 0.0014, 0.0022, 0.003\}$ for dust. For each combination of (k_0, SAE) , the standard sub-LUT is computed for 8 AOD_{443} nodes $\{0.2, 0.5, 0.8, 1.2, 1.8, 2.8, 4.2, 6.\}$, $18 \text{ values of cosine of solar and view zenith angle from 0.15 to 1 with step 0.05, and 5 azimuths for the range <math>160^{\circ}-180^{\circ}$ with step 5° . The sub-LUT is computed for 2 relative pressure levels, $P = 1 \ (1,013.25 \ \text{mB})$ and 0.7, for the surface height interpolation.

Calculation of TOA reflectance for each nodal combination ($k_{0,i}$, SAE_{i} , AOD_{n}) involves 4D-interpolation in view geometry and surface pressure/height. Generating output for an arbitrary set of parameters (k_{0} , SAE, AOD) involves further tri-linear interpolation over the respective nodes. The partial derivatives over these parameters are also estimated using the neighbor nodes. Despite this rather crude estimation of partial derivatives, the algorithm features fast convergence on average within ~1–3% of the measurements. Overall, the developed LUT-based approach is numerically optimized and very efficient, resulting only in a fractional increase of the processing time compared to the standard MAIAC EPIC algorithm.

As the retrieval results depend on the assumed aerosol height, the v2 algorithm reported results for two cases with ALH = 1 km and 4 km, which generally represent the boundary layer aerosol and the long-range transport. The described algorithm was applied when ${\rm AOD}_{443}$ retrieved with the background aerosol model exceeded 0.6 or when absorbing smoke or dust were detected (Lyapustin et al., 2021b).

2.3 MAIAC v3 algorithm: including ALH retrieval

The design of EPIC, with channels in the UV, visible, and in the atmospheric oxygen A and B-bands, gives a good sensitivity to the height of aerosol layer. The O_2 B (688 nm) and O_2 A (764 nm) bands from EPIC have been used to retrieve ALH and AOD both over the water (Xu X. et al., 2017) and the land (Xu et al., 2019) by combining oxygen bands with different weights. Compared to O2 B-band, the A-band has a stronger absorption and better sensitivity to ALH over the water. Over land, the surface is bright in the near-IR and AOD rapidly decreases with wavelength in case of smoke aerosol with small particle size. These compounding factors generally limit the use of the O_2 A-band for ALH retrieval over land except for optically thick conditions (e.g., Xu et al., 2016).

On the other hand, the UV-vis measurements of EPIC provide a complementary ALH sensitivity for the absorbing aerosols such as smoke and dust. At 340 and 388 nm the surface is dark, and the atmospheric optical depth is high due to both Rayleigh and aerosol, in particular fine mode, contributions. The high optical depth results

in high multiple scattering which effectively dims the reflected intensity from the aerosol layer compared to the non-absorbing aerosol case. To the first approximation, a combination of this reduction with compensating contribution from the non-absorbing Rayleigh atmosphere above the aerosol layer leads to the ALH-dependence of the reflected intensity in the UV.

In the v3 algorithm, we combine the UV-vis-NIR and O2 A,B-bands of EPIC to simultaneously retrieve four parameters including ALH:

$$F^{2} = \frac{1}{N} \sum \left[\frac{L_{\lambda}^{m} - L_{\lambda}^{t}}{\sigma_{\lambda} L_{\lambda}^{m}} \right]^{2} = min \{ AOD_{443}, k_{0}, SAE, ALH \}, \quad (3)$$

where the superscript 'm' stands for the measurement and 't' is for theoretical, or simulated, value.

From a technical standpoint, the v3 algorithm uses the v2 LUTs generated for four aerosol layer heights (0.5, 1, 4, 7 km) and adds interpolation in ALH. We model aerosol profile as a 2 km layer which is centered at ALH and has 95% of loading. The remaining 5% of aerosol is placed either below (ALH = 4, 7 km) or above (ALH = 0.5, 1 km). In case of the shallow boundary layer aerosol (ALH = 0.5 km), the geometrical thickness of aerosol layer is 1 km.

The O₂ bands are accommodated using a separate look-up table generated using the Spherical Harmonics Interpolation and Profile Correction (SHARM-IPC) code for numerical simulation of multiple scattering of sunlight (Lyapustin, 2003). The SHARM-IPC code is similar to the correlated-k algorithm (Goody et al., 1989; Hogan and Matricardi, 2020) but offers a better accuracy and arbitrary spectral resolution at similarly high speed. It uses a line-by-line (LBL) approach to compute direct atmospheric transmittance and single scattering path radiance, and correlatedk approach to compute multiple scattering path radiance (LMS), diffuse atmospheric transmittance, and spherical albedo of atmosphere. LMS is further corrected line-by-line for the difference between the average vertical profile in bins of the gaseous absorption optical thickness and specific vertical profile at a given wavenumber (Lyapustin, 2003). The computations are performed at 0.01 cm⁻¹ spectral resolution. We are using the Coddington et al. (2023) solar irradiance model and the latest HITRAN-2020 (Gordon et al., 2022) spectroscopy, simulated using our tool for LBL absorption spectroscopy (Korkin et al., 2025), and with continuum models for O2, NO2, CO2 (Clough et al., 2005), and O₂-O₂ and O₂-air collision over 300–650 nm region (Thalman and Volkamer, 2013; Karman et al., 2019; Finkenzeller and Volkamer, 2022).

The calibration of the UV (Herman et al., 2018; Huang and Yang, 2022), visible and NIR (Geogdzhayev and Marshak, 2018; Doelling et al., 2019; Geogdzhayev et al., 2021) and O_2 (Geogdzhayev and Marshak, 2018) EPIC bands is performed using different techniques. There are indications of a possible calibration bias in the O_2 -A band (Zhou et al., 2023; Lu et al., 2021). For this reason, the v3 retrieval consists of two steps: 1) The v3 minimization (Equation 3) provides ALH, which is used in 2) the v2 minimization (Equation 2) providing the aerosol properties $\{AOD_{443}, k_0, SAE\}$. Extensive global multi-year validation of aerosol AOD and spectral single scattering albedo shows that such 2-step approach results in a better accuracy of the aerosol properties.

Compared to the v2 inversions, which were limited to $AOD_{443} > 0.6$, the v3 inversions are applied to a wider range of aerosol optical depths, $AOD_{443} > 0.4$. Note that both MAIAC v2 and v3 assume aerosol size distribution and real refractive index, and apply for regions with pure biomass burning or dust. A proper handling of cases with mixed dust and biomass burning, prevalent, for instance, in sub-Saharan Africa, will require further development.

The v3 algorithm has been applied to re-process the entire EPIC record of observations using computational resources of the NASA Center for Climate Simulations.

3 Aerosol height retrieval examples

We illustrate MAIAC v3 ALH retrievals from EPIC with respect to the measurements of the Cloud-Aerosol Lidar with Orthogonal Polarization (CALIOP) on board the Cloud-Aerosol Lidar and Infrared Pathfinder Satellite Observations (CALIPSO) satellite. CALIPSO was operational for 17 years until August 2023 providing global measurements of aerosol vertical distribution. We collected profiles of total attenuated backscatter coefficients at 532 nm (β; units of km⁻¹ sr⁻¹) from the CALIPSO Lidar Level 2 Aerosol Profile version 4.51 dataset (CAL_LID_L2_ 05kmAPro-Standard-V4-51) for the missions' overlap period of 2015-2023. As a measure of aerosol profile integral value, we are using the backscatter-weighted aerosol layer height ALH_C = $\sum z\beta$ / $\sum \beta$, where z is the height of each layer. This common definition is widely used to validate aerosol layer height using CALIOP (e.g., Nanda et al., 2020; Kim et al., 2025). We use all ALH_C data at 5 km horizontal (along-track) resolution, matched to MAIAC EPIC data located within 20 km of CALIOP measurements and within ± 30 min of EPIC acquisitions. Since EPIC data are 2 × 2 8 km pixels aggregated onboard, the EPIC footprint size at nadir is 16 km, and thus aggregation within 20 km distance from CALIOP better represents true EPIC resolution than the over-sampled 10 km of MAIAC EPIC grid. For global comparisons with CALIOP, the Sun and view zenith angles of EPIC are limited to <63.3°. To mitigate the ALH uncertainty for low aerosol-loading cases, we set a threshold of CALIOP AOD $_{532} \ge 0.6$. Finally, MAIAC ALH is defined with respect to the sea level.

Figure 1 shows six different cases of v3 MAIAC EPIC ALH retrievals overlaid on CALIOP curtain plots (left). The scatterplot comparisons for each case are shown on the right. On the left plots, MAIAC ALH is presented by the brown circles and yellow triangles for smoke and mineral dust, respectively, while the CALIOP ALH_C is given by the green circles. The first three panels (a-c) present the biomass burning aerosol cases, the second two panels (d-e) show cases of mineral dust both over the land and the ocean, and the last one (e) contains both dust off the western Africa over land transitioning to transported biomass burning aerosol over the Atlantic ocean. The associated geographic maps of MAIAC AOD₄₄₃, SSA₄₄₃ and ALH along with matching CALIPSO ground track (red line) are displayed in Figure 2.

In general, ALH for the biomass burning aerosols has a strong regional pattern. This pattern is defined by the fuel characteristics and type of burning (van der Werf et al., 2017; Val Martin et al., 2010). For instance, active flaming forest wildfires at northern latitudes often have significant thermal energy to loft smoke up

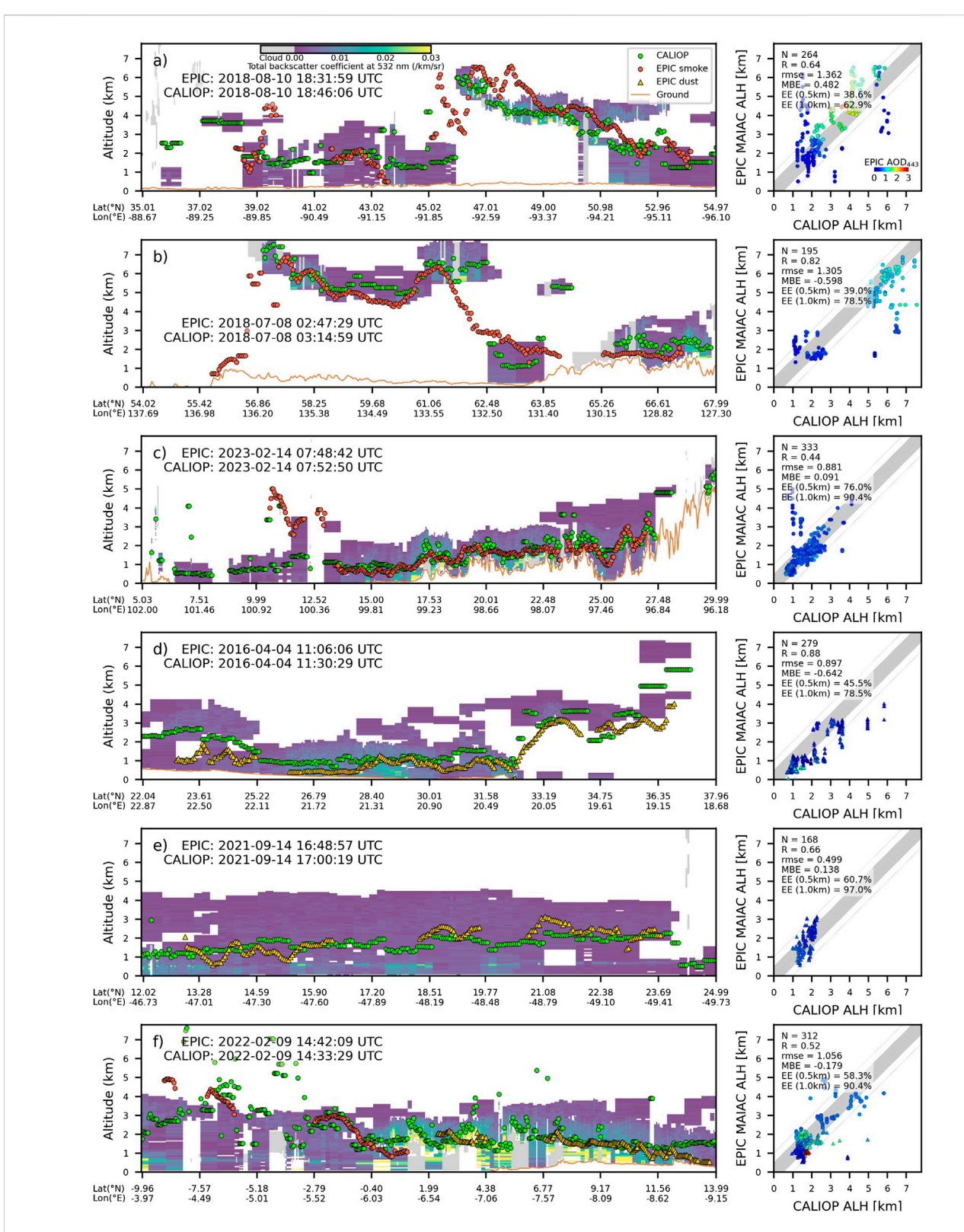


FIGURE 1 Illustration of global v3 MAIAC EPIC ALH retrievals for different world regions and aerosol types along with matching CALIOP data (cases (a-f)). The curtains show the CALIOP aerosol backscatter coefficient (β_{532}). The grey color indicates detected clouds, and the yellow line at the bottom shows the surface height profile. The EPIC ALH is given by brown circles for smoke and by yellow triangles for dust; green circles represent CALIOP backscatter extinction weighted ALH_C. The respective scatterplots on the right summarize assessment of MAIAC ALH accuracy for individual cases of smoke (circles) and dust (triangles). The color of symbols corresponds to MAIAC EPIC AOD₄₄₃. The color bar scale of the curtain plots is displayed on the top panel.

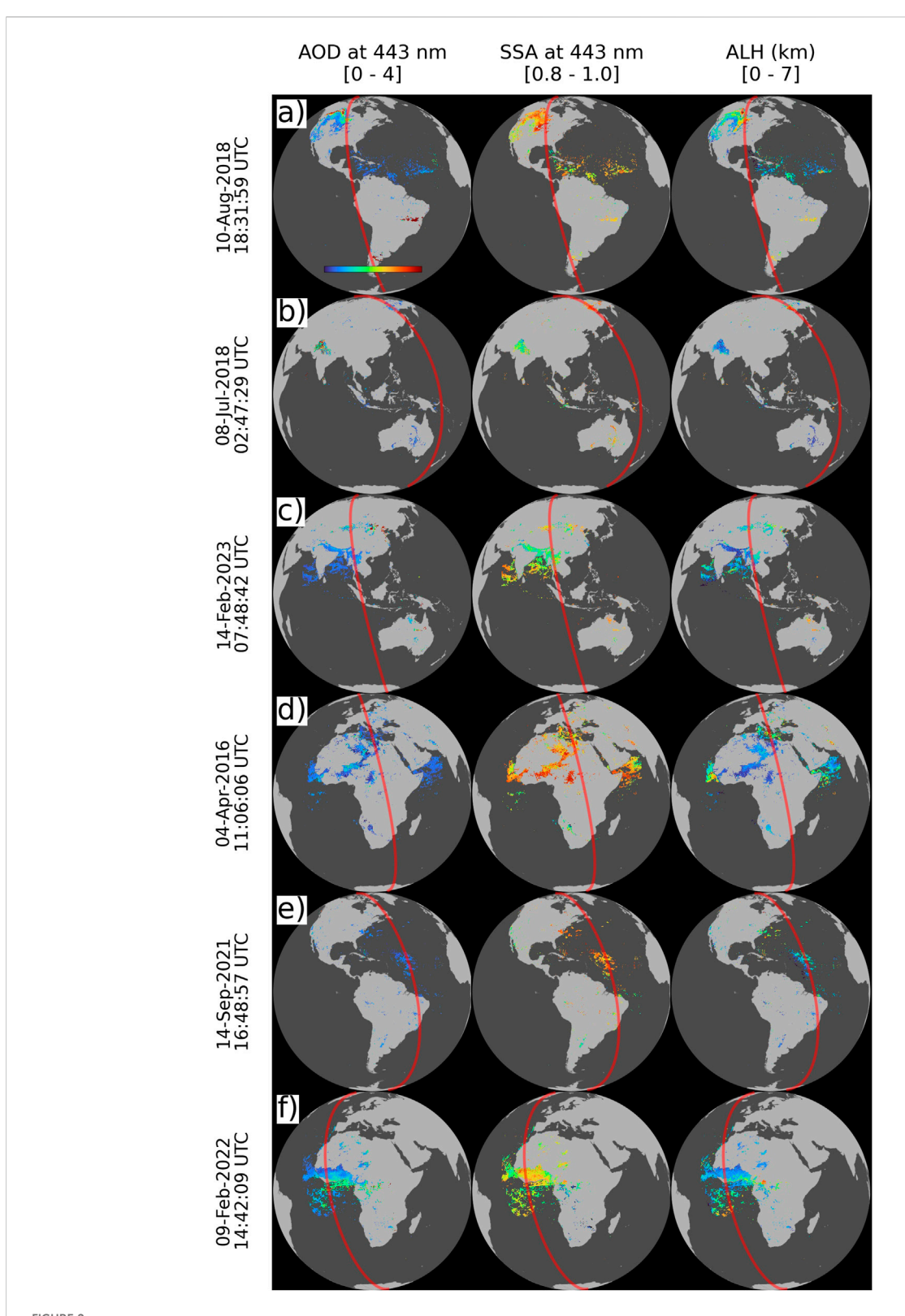
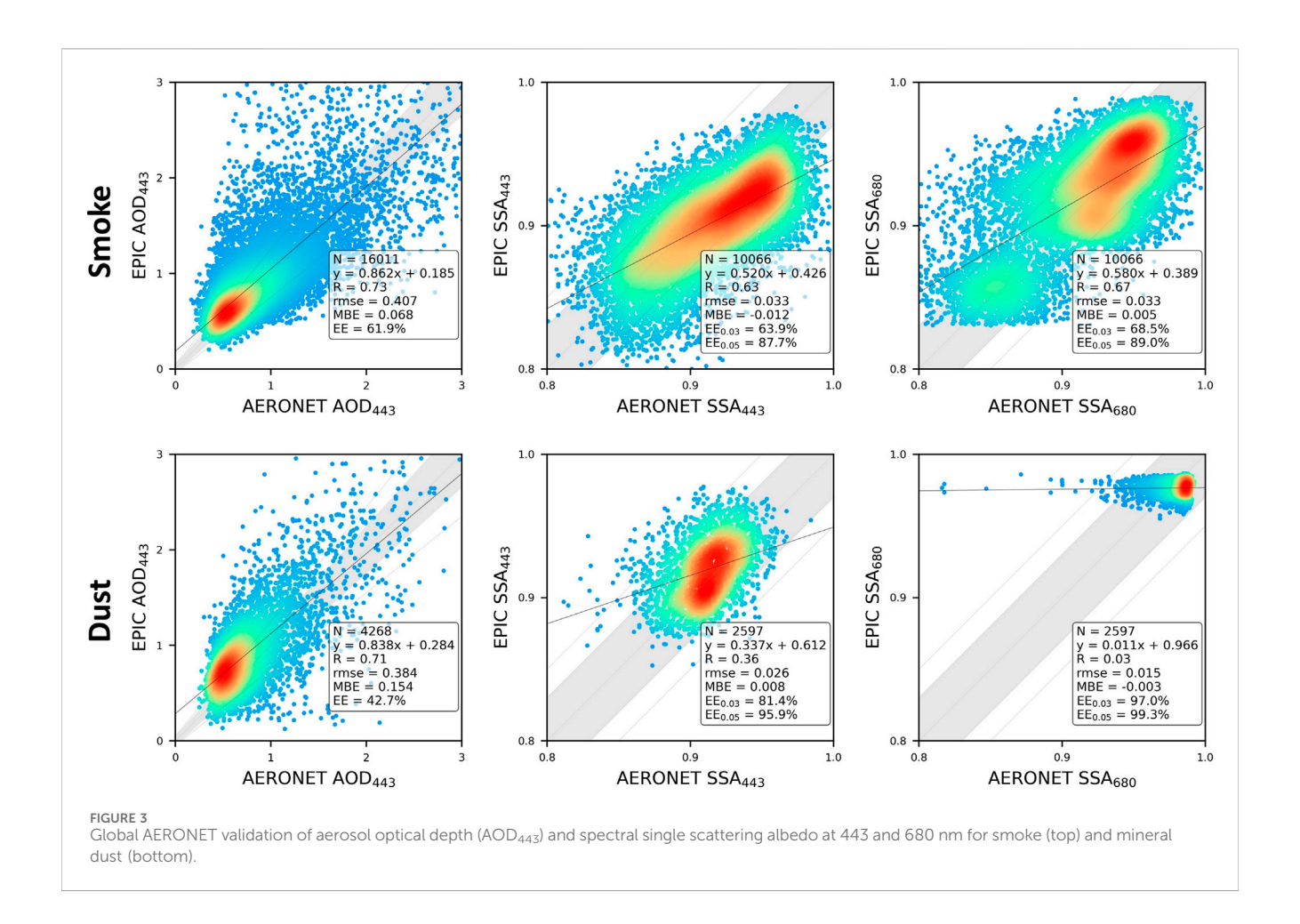


FIGURE 2 Geographic maps of AOD₄₄₃, SSA₄₄₃ and ALH showing the v3 MAIAC EPIC retrievals for cases presented in Figure 1 (cases (a-f)). The red line shows the matching CALIPSO ground track within ± 30 min. The rainbow color bar scale, shown in the top left image, is common to all plots but with different ranges for AOD [0-4], SSA [0.8-1] and ALH [0-7 km].



to 7 km altitude and higher. Panels (a)-(b) show two examples of properties of smoke generated by forest wildfires in Canada and northwestern United States, and in Siberia in July-August 2018. In both cases, the retrieved ALH corresponds well to the reference $ALH_{\rm C}$ in the full range of altitudes up to 7 km. In second typical pattern, the emission sources may include residential cooking and heating, transportation, industry and energy sectors, grasslands or sparse vegetation fires, and generate smoke typically constrained to the atmospheric boundary layer. An example of such case for the south Asia transect is given in panel (c). In this case, the aerosol height stays within $\sim 1-3$ km.

The EPIC ALH retrieval pattern has a good spatial consistency, though sometimes significant outliers can be found usually over brighter surface regions with low aerosol opacity, e.g., over 45°–46° Lat in panel (a) and over 64° Lat in panel (b). A significant growth of EPIC footprint, by a factor of ~1/cos²(Lat), may increase error of matching CALIOP-EPIC geolocation, and enhance probability of undetected subpixel clouds by MAIAC EPIC, both factors potentially contributing to high ALH errors. In panel (c), both MAIAC and CALIOP detected elevated aerosol layer at 4–5 km altitude at ~11° Lat as seen from the curtain plot, though these points did not enter the scatterplot on the right due to a small geographic displacement, possibly caused by the geolocation error.

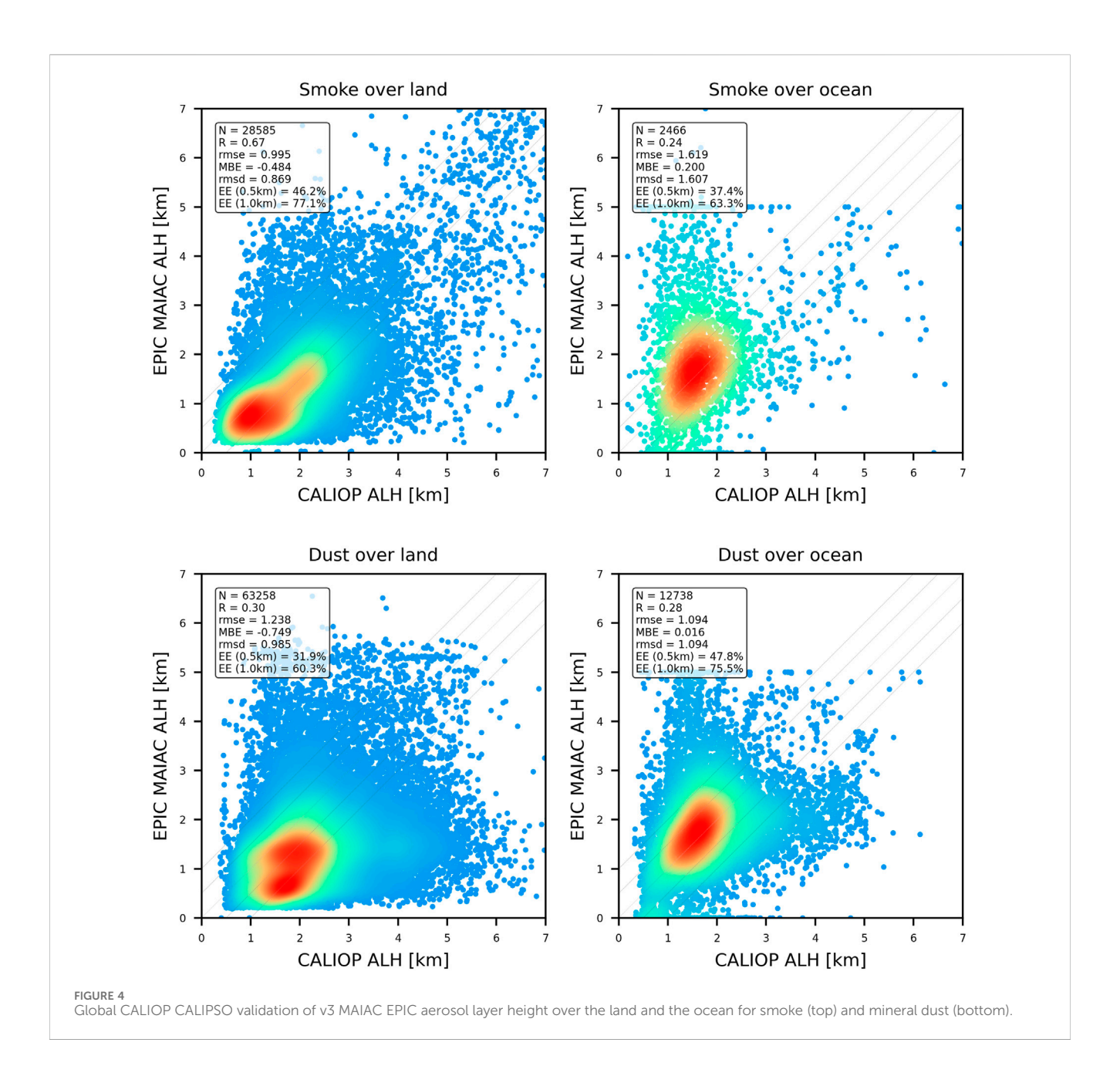
Two cases of African dust are shown in panels (d-e). In panel (d), EPIC data show that dust aerosol stays within 1–2 km from the surface over northern Africa, but rises to altitudes of 3–4 km over the

Mediterranean sea. The collocated CALIOP data confirm MAIAC EPIC ALH up to 36° Lat, but show higher dust elevations by 1–2 km for the 36°–37° Lat part of the track. Panel (e) shows south-north transect of Saharan dust transported over Atlantics. In this case, EPIC ALH not only closely matches ALH $_{\rm C}$ but also shows a systematic reduction in layer height from north to south of the dust plume.

Finally, in panel (f) the CALIOP path transects, first, the south-African smoke over Atlantics south of the equator, and then the Saharan dust initially over Atlantics and then over the western Sahara. EPIC retrievals nearly perfectly match CALIOP for both smoke and dust cases. Both data show rising ALH from ~1 km to 2 km for dust at $14^{\circ}-2^{\circ}$ Lat north of equator, and rise of biomass burning aerosol over Atlantics from 1 to 2 km on the equator to 4–5 km south of equator at ~ -10° Lat.

4 Validation

The previous selected examples demonstrated that the v3 MAIAC EPIC algorithm provides reliable ALH retrievals with good accuracy. Validation statistics presented in scatterplots of Figure 1 allows us to make preliminary conclusions about ALH accuracy. For instance, the *RMSE* is proportional to the total range of ALH variation staying within 0.5–1 km for aerosols within the boundary layer and increasing to 1–1.5 km for smoke reaching the



free troposphere. The *bias* for the entire transects on average is within approximately ± 0.5 km though it can reach several km for conditions when aerosol loading is low and/or the surface is bright. The expected error (*EE*) in the presented cases can be assessed as *EE* ~ 1 km when over $\sim 67\%$ of ALH retrievals stay within 1 km from the reference CALIOP values.

To yield a globally representative accuracy assessment, we used a 2015-2024 EPIC data record re-processed with v3 MAIAC algorithm and performed validation of derived aerosol optical properties and layer height using AERONET and CALIOP (up to August 2023) data, respectively. The details of ALH validation using CALIOP were described above in Section 3. For optical properties validation we used AERONET version 3 (Giles et al., 2019) Level 1.5 AOD and inversion data. MAIAC EPIC AOD₄₄₃ data were limited to cosines of view and solar zenith angles above 0.45. We used an average MAIAC AOD collocated in space and time within

25 km distance and ± 30 min for all AERONET stations, respectively. To filter cloudy conditions, we required successful retrievals for more than 50% the collocated pixels in the 50 \times 50 km² box.

To increase the number of EPIC-AERONET matchups for SSA, the temporal window was increased to ± 3 h. Additional constraints on AERONET AOD (AOD₄₄₀ > 0.6) and AERONET Angstrom Exponent (AE) were applied to separate smoke (AE > 0.4) from dust (AE<0.4).

The MAIAC expected error for AOD is defined as $EE = \pm (0.05 + 0.2 \times \text{AERONET AOD})$ for AOD₄₄₃ and as ± 0.03 for the single scattering albedo, which is the stated uncertainty of AERONET inversion-based SSA (Sinyuk et al., 2020).

The results from validation analysis are summarized below in Figures 3, 4. They are presented separately for smoke and dust cases. Figure 3 shows that the v3 algorithm retrieves aerosol optical

properties with good accuracy. The AOD has a correlation

coefficient $R \sim 0.71$ -0.73 and $RMSE \sim 0.4$. The mean AOD bias is positive for both smoke (0.07) and dust (0.15). Partly responsible for this bias is the EPIC view geometry near the exact backscattering, where the surface brightness increases often significantly due to the lack of shadows (called 'hot spot', e.g., Ross and Marshak, 1989). While the AOD retrieval accuracy is average, the achieved global accuracy of spectral absorption is very good. The SSA correlates well with AERONET values, in particular for smoke (R \sim 0.63-0.67), and shows low $RMSE \sim 0.02$ -0.03 and constrained mean bias within approximately ± 0.01 . Importantly, about 64%-69%/81%-97% of SSA values for smoke/dust aerosols match AERONET SSA within uncertainty of ± 0.03 . These results are similar to those achieved by the POLDER GRASP (Chen et al., 2020) despite the lack of multiangle and polarization information in EPIC and generally unfavorable view geometry for aerosol characterization.

A global CALIOP-based validation of MAIAC EPIC ALH, based on the entire EPIC-CALIPSO overlap period of July 2015 – August 2023, is shown in Figure 4. The results are displayed separately for smoke and dust aerosols over the land and over the ocean. While ALH displays a strong regional dependence related to different fuel types and fire energy, as was mentioned previously, here we focus on a global accuracy analysis and detailed regional analysis will be given elsewhere. Figure 4 shows that the v3 algorithm offers reliable ALH with good accuracy: it has a low global negative bias of $-0.45 \, \mathrm{km}$ for smoke and $-0.75 \, \mathrm{km}$ for dust over land, no bias over the ocean, and RMSE $\sim 1.1 \, \mathrm{km}$. The bias may reflect the difference between EPIC ALH representing optical centroid, and backscatter-weighted mean height from CALIOP.

The expected error was assessed for two values of ALH accuracy of 0.5 km and 1 km. From 46% over land to 37% over water of retrieved ALH for smoke fall within 0.5 km of CALIOP data, while for global dust these values are 32% and 48%, respectively. The true expected error, defined for $2\sigma \sim 67\%$ of retrievals within the "validation truth" for the gaussian error distribution, is closer to 1 km for the global data. For instance, between 77% over land and 63% over ocean of smoke ALH values are within $EE = \pm 1$ km from CALIOP ALH_C. The numbers are similar for dust, from 60% over land to 75.5% over ocean are within $EE = \pm 1$ km.

5 Summary

A detailed aerosol characterization including microphysical properties requires high information content available from multi-angle, multi-spectral, and ideally polarimetric observations. Here, we presented a new v3 MAIAC algorithm that simultaneously retrieves AOD, ALH and spectral absorption from the single-look EPIC imager. Performed global validation against AERONET shows only a moderate accuracy of MAIAC EPIC AOD with $R \sim 0.71$ -0.73, RMSE \sim 0.4, and EE \sim 20% which is mostly due to the unfavorable backscattering view geometry and partly due to the coarse spatial resolution. At the same time, due to the EPIC's UV channels with reduced sensitivity to the surface reflectance, the achieved accuracy of the single scattering albedo at 443 and 680 nm is very good, with RMSE ~ 0.02-0.03, bias within approximately ± 0.01 , and 64%-97%of SSA values within expected error of ± 0.03 . Such a high accuracy of retrievals allowed us to develop and implement composition analysis of absorbing aerosol components, focusing on hematite and goethite in mineral dust (Go et al., 2022), and on black and brown carbon in smoke (Choi et al., 2024). Column volumetric fractions and mass concentrations of these components are reported in the MAIAC EPIC atmospheric product suite along with derived aerosol optical properties (AOD, k₀, SAE) and single scattering albedo at 340, 388, 443, 680 nm. Concentrations of absorbers is an important input for the chemical transport models and for derivation of speciated particulate matter for health exposure research.

ALH is in integral representation of the aerosol profile. Global satellite-based ALH can be used to constrain plume injection height in models and to improve predictions of the fine particulate matter (PM_{2.5}) concentration near the surface (e.g., Lu et al., 2021). CALIOP validation shows that the v3 MAIAC EPIC ALH correlates well, in particular for smoke, with the backscatterweighted height. The ALH is lower than CALIOP ALHC by 0.45-0.75 km over land but shows no bias over the ocean, and has $RMSE \sim 1.1$ km and 60%–77% of retrievals within $EE = \pm 1$ km. EPIC-based retrievals are global and provide ALH values for regions with elevated aerosol loading (AOD $_{443}$ > 0.4) both near the emission source and far away in the transported regime. This approach solves the problem of a limited coverage by our previously developed thermal technique for the wildfire aerosol injection height retrieval which was limited to ~100 km proximity to the source of the active burning (Lyapustin et al., 2020).

An assumption of aerosol type (background, smoke or dust), size distribution and real refractive index is a current limitation of our approach. This limitation can be resolved with future research to add a virtual multi-angle capability through combining EPIC with other passive sensors collocated in space and time.

Data availability statement

The datasets presented in this study can be found in online repositories. The names of the repository/repositories and accession number(s) can be found below: Atmospheric Science Data Center (ASDC) at NASA Langley Research Center (Available at: https://doi.org/10.5067/EPIC/DSCOVR/L2_MAIAC.002).

Author contributions

AL: Conceptualization, Funding acquisition, Investigation, Methodology, Software, Supervision, Writing – original draft, Writing – review and editing. MC: Investigation, Software, Validation, Visualization, Writing – review and editing. YW: Data curation, Formal Analysis, Software, Writing – review and editing. SK: Formal Analysis, Methodology, Software, Writing – review and editing. EH: Conceptualization, Methodology, Writing – review and editing. AM: Funding acquisition, Project administration, Supervision, Writing – review and editing.

Funding

The author(s) declare that financial support was received for the research and/or publication of this article. This work was

supported by the NASA DSCOVR program, NASA PACE program (19-PACESAT19-0039) and by the Office of Naval Research.

Acknowledgments

We are grateful to the AERONET team for providing validation data and to the NASA Center for Climate Simulations providing resources for EPIC data processing. E. Hyer's contribution was supported by the Office of Naval Research Code 32.

Conflict of interest

The authors declare that the research was conducted in the absence of any commercial or financial relationships that could be construed as a potential conflict of interest.

References

Bond, T. C. (2001). Spectral dependence of visible light absorption by carbonaceous particles emitted from coal combustion. *Geophys. Res. Lett.* 28, 4075–4078. doi:10.1029/2001GL013652

Boucher, O., Randall, D., Artaxo, P., Bretherton, C., Feingold, G., Forster, P., et al. (2013). "Clouds and aerosols," in Climate change 2013 – the physical science basis: Working group I contribution to the fifth assessment report of the intergovernmental panel on climate change (Cambridge University Press), 571–658. doi:10.1017/CBO9781107415324.016

Chen, C., Dubovik, O., Fuertes, D., Litvinov, P., Lapyonok, T., Lopatin, A., et al. (2020). Validation of GRASP algorithm product from POLDER/PARASOL data and assessment of multi-angular polarimetry potential for aerosol monitoring. *Earth Syst. Sci. Data* 12, 3573–3620. doi:10.5194/essd-12-3573-2020

Chen, X., Wang, J., Xu, X., Zhou, M., Zhang, H., Castro Garcia, L., et al. (2021). First retrieval of absorbing aerosol height over dark target using TROPOMI oxygen B band: algorithm development and application for surface particulate matter estimates. *Remote Sens. Environ.* 265, 112674. doi:10.1016/j.rse.2021.112674

Chen, C., Lei, X., Liu, Z., Gu, H., Dubovik, O., Litvinov, P., et al. (2025). Development of level 2 aerosol and surface products from cross-track scanning polarimeter POSP on board the GF-5(02) satellite. *Earth Syst. Sci. Data* 17, 3497–3519. doi:10.5194/essd-17-3497-2025

Choi, M., Lyapustin, A., Schuster, G. L., Go, S., Wang, Y., Korkin, S., et al. (2024). Light-absorbing black carbon and brown carbon components of smoke aerosol from DSCOVR EPIC measurements over North America and central Africa. Atmos. Chem. Phys. 24, 10543–10565. doi:10.5194/acp-24-10543-2024

Clough, S. A., Shephard, M. W., Mlawer, E. J., Delamere, J. S., Iacono, M. J., Cady-Pereira, K., et al. (2005). Atmospheric radiative transfer modeling: a summary of the AER codes. *J. Quant. Spectrosc. Radiat. Transf.* 91, 233–244. doi:10.1016/j.jqsrt.2004. 05.058

Coddington, O. M., Richard, E. C., Harber, D., Pilewskie, P., Woods, T. N., Snow, M., et al. (2023). Version 2 of the TSIS-1 hybrid solar reference spectrum and extension to the full spectrum. *Earth Sp. Sci.* 10, e2022EA002637. doi:10.1029/2022EA002637

de Graaf, M., Sneep, M., ter Linden, M., Tilstra, L. G., Donovan, D. P., van Zadelhoff, G.-J., et al. (2025). Improvements in aerosol layer height retrievals from TROPOMI oxygen A-band measurements by surface albedo fitting in optimal estimation. *Atmos. Meas. Tech.* 18, 2553–2571. doi:10.5194/amt-18-2553-2025

Diner, D. J., Boland, S. W., Brauer, M., Bruegge, C., Burke, K. A., Chipman, R., et al. (2018). Advances in multiangle satellite remote sensing of speciated airborne particulate matter and association with adverse health effects: from MISR to MAIA. *J. Appl. Remote Sens.* 12 (4), 1. doi:10.1117/1.JRS.12.042603

Doelling, D., Haney, C., Bhatt, R., Scarino, B., and Gopalan, A. (2019). The intercalibration of the DSCOVR EPIC imager with aqua-MODIS and NPP-VIIRS. *Remote Sens.* 11 (13), 1609. doi:10.3390/rs11131609

Dubovik, O., Holben, B., Eck, T. F., Smirnov, A., Kaufman, Y. J., King, M. D., et al. (2002). Variability of absorption and optical properties of key aerosol types observed in worldwide locations. *J. Atmos. Sci.* 59, 590–608. doi:10.1175/1520-0469(2002) 059<0590:VOAAOP>2.0.CO:2

Generative AI statement

The author(s) declare that no Generative AI was used in the creation of this manuscript.

Any alternative text (alt text) provided alongside figures in this article has been generated by Frontiers with the support of artificial intelligence and reasonable efforts have been made to ensure accuracy, including review by the authors wherever possible. If you identify any issues, please contact us.

Publisher's note

All claims expressed in this article are solely those of the authors and do not necessarily represent those of their affiliated organizations, or those of the publisher, the editors and the reviewers. Any product that may be evaluated in this article, or claim that may be made by its manufacturer, is not guaranteed or endorsed by the publisher.

Dubovik, O., Sinyuk, A., Lapyonok, T., Holben, B. N., Mishchenko, M., Yang, P., et al. (2006). Application of spheroid models to account for aerosol particle nonsphericity in remote sensing of desert dust. *J. Geophys. Res. Atmos.* 111, 2005JD006619–34. doi:10.1029/2005JD006619

Dubovik, O., Herman, M., Holdak, A., Lapyonok, T., Tanré, D., Deuzé, J. L., et al. (2011). Statistically optimized inversion algorithm for enhanced retrieval of aerosol properties from spectral multi-angle polarimetric satellite observations. *Atmos. Meas. Tech.* 4, 975–1018. doi:10.5194/amt-4-975-2011

Dubovik, O., Li, Z., Mishchenko, M. I., Tanré, D., Karol, Y., Bojkov, B., et al. (2019). Polarimetric remote sensing of atmospheric aerosols: instruments, methodologies, results, and perspectives. *J. Quant. Spectrosc. Radiat. Transf.* 224, 474–511. doi:10. 1016/j.jqsrt.2018.11.024

Finkenzeller, H., and Volkamer, R. (2022). O₂–O₂ CIA in the gas phase: cross-section of weak bands, and continuum absorption between 297–500 nm. *J. Quant. Spectrosc. Radiat. Transf.* 279, 108063. doi:10.1016/j.jqsrt.2021.108063

Fu, G., Rietjens, J., Laasner, R., van der Schaaf, L., van Hees, R., Yuan, Z., et al. (2025). Aerosol retrievals from SPEXone on the NASA PACE Mission: first results and validation. *Geophys. Res. Lett.* 52, e2024GL113525. doi:10.1029/2024GL113525

Geogdzhayev, I. V., and Marshak, A. (2018). Calibration of the DSCOVR EPIC visible and NIR channels using MODIS Terra and aqua data and EPIC lunar observations. *Atmos. Meas. Tech.* 11, 359–368. doi:10.5194/amt-11-359-2018

Geogdzhayev, I. V., Marshak, A., and Alexandrov, M. (2021). Calibration of the DSCOVR EPIC visible and NIR channels using multiple LEO radiometers. *Front. Remote Sens.* 2, 671933. doi:10.3389/frsen.2021.671933

Giles, D. M., Sinyuk, A., Sorokin, M. G., Schafer, J. S., Smirnov, A., Slutsker, I., et al. (2019). Advancements in the aerosol robotic network (AERONET) version 3 database – automated near-real-time quality control algorithm with improved cloud screening for sun photometer aerosol optical depth (AOD) measurements. *Atmos. Meas. Tech.* 12, 169–209. doi:10.5194/amt-12-169-2019

Go, S., Lyapustin, A., Schuster, G. L., Choi, M., Ginoux, P., Chin, M., et al. (2022). Inferring iron-oxide species content in atmospheric mineral dust from DSCOVR EPIC observations. *Atmos. Chem. Phys.* 22, 1395–1423. doi:10.5194/acp-22-1395-2022

Goody, R., West, R., Chen, L., and Crisp, D. (1989). The correlated-k method for radiation calculations in nonhomogeneous atmospheres. *J. Quant. Spectrosc. Radiat. Transf.* 42, 539–550. doi:10.1016/0022-4073(89)90044-7

Gordon, I. E., Rothman, L. S., Hargreaves, R. J., Hashemi, R., Karlovets, E. V., Skinner, F. M., et al. (2022). The HITRAN2020 molecular spectroscopic database. *J. Quant. Spectrosc. Radiat. Transf.* 277, 107949. doi:10.1016/j.jqsrt.2021.107949

Hasekamp, O. P., Fu, G., Rusli, S. P., Wu, L., Di Noia, A., Brugh, J., et al. (2019). Aerosol measurements by SPEXone on the NASA PACE mission: expected retrieval capabilities. *J. Quant. Spectrosc. Radiat. Transf.* 227, 170–184. doi:10.1016/j.jqsrt.2019. 02.006

Herman, J., Huang, L., McPeters, R., Ziemke, J., Cede, A., and Blank, K. (2018). Synoptic ozone, cloud reflectivity, and erythemal irradiance from sunrise to sunset for the whole earth as viewed by the DSCOVR spacecraft from the earth-sun Lagrange 1 orbit. *Atmos. Meas. Tech.* 11, 177–194. doi:10.5194/amt-11-177-2018

- Hogan, R. J., and Matricardi, M. (2020). Evaluating and improving the treatment of gases in radiation schemes: the Correlated K-Distribution model intercomparison project (CKDMIP). *Geosci. Model Dev.* 13, 6501–6521. doi:10.5194/gmd-13-6501-2020
- Holben, B. N., Eck, T. F., Slutsker, I., Tanré, D., Buis, J. P., Setzer, A., et al. (1998). AERONET—A federated instrument network and data archive for aerosol characterization. *Remote Sens. Environ.* 66, 1–16. doi:10.1016/S0034-4257(98)00031-5
- Huang, X., and Yang, K. (2022). Algorithm theoretical basis for ozone and sulfur dioxide retrievals from DSCOVR EPIC. *Atmos. Meas. Tech.* 15, 5877–5915. doi:10.5194/amt-15-5877-2022
- Karman, T., Gordon, I. E., van der Avoird, A., Baranov, Y. I., Boulet, C., Drouin, B. J., et al. (2019). Update of the HITRAN collision-induced absorption section. *Icarus* 328, 160–175. doi:10.1016/j.icarus.2019.02.034
- Kim, H., Chen, X., Wang, J., Lu, Z., Zhou, M., Carmichael, G. R., et al. (2025). Aerosol layer height (ALH) retrievals from oxygen absorption bands: intercomparison and validation among different satellite platforms, GEMS, EPIC, and TROPOMI. *Atmos. Meas. Tech.* 18, 327–349. doi:10.5194/amt-18-327-2025
- Kirchstetter, T. W., Novakov, T., and Hobbs, P. V. (2004). Evidence that the spectral dependence of light absorption by aerosols is affected by organic carbon. *J. Geophys. Res. Atmos.* 109, 2004JD004999–12. doi:10.1029/2004JD004999
- Kondragunta, S., Laszlo, I., Zhang, H., Ciren, P., and Huff, A. (2020). "Air quality applications of ABI aerosol products from the GOES-R series," in *The GOES-R series* (Elsevier), 203–217. doi:10.1016/B978-0-12-814327-8.00017-2
- Korkin, S., and Lyapustin, A. (2023). Radiative interaction of atmosphere and surface: write-up with elements of code. *J. Quant. Spectrosc. Radiat. Transf.* 309, 108663. doi:10. 1016/j.jqsrt.2023.108663
- Korkin, S., Sayer, A. M., Ibrahim, A., and Lyapustin, A. (2025). A practical guide to coding line-by-line trace gas absorption in Earth's atmosphere. *J. Quant. Spectrosc. Radiat. Transf.* 337, 109345. doi:10.1016/j.jqsrt.2025.109345
- Lee, J., Hsu, N. C., Kim, W. V., Sayer, A. M., and Tsay, S. (2024). VIIRS version 2 deep blue aerosol products. *J. Geophys. Res. Atmos.* 129, e2023JD040082. doi:10.1029/2023JD040082
- Levy, R. C., Mattoo, S., Munchak, L. A., Remer, L. A., Sayer, A. M., Patadia, F., et al. (2013). The collection 6 MODIS aerosol products over land and ocean. *Atmos. Meas. Tech.* 6, 2989–3034. doi:10.5194/amt-6-2989-2013
- Li, L., Dubovik, O., Derimian, Y., Schuster, G. L., Lapyonok, T., Litvinov, P., et al. (2019). Retrieval of aerosol components directly from satellite and ground-based measurements. *Atmos. Chem. Phys.* 19, 13409–13443. doi:10.5194/acp-19-13409-2019
- Li, L., Che, H., Zhang, X., Chen, C., Chen, X., Gui, K., et al. (2022). A satellite-measured view of aerosol component content and optical property in a haze-polluted case over north China plain. *Atmos. Res.* 266, 105958. doi:10.1016/j.atmosres.2021.105958
- Lu, Z., Wang, J., Xu, X., Chen, X., Kondragunta, S., Torres, O., et al. (2021). Hourly mapping of the layer height of thick smoke plumes over the Western U.S. in 2020 severe fire season. *Front. Remote Sens.* 2, 766628. doi:10.3389/frsen.2021.766628
- Lyapustin, A. I. (2003). Interpolation and profile correction (IPC) method for shortwave radiative transfer in spectral intervals of gaseous absorption. *J. Atmos. Sci.* 60, 865–871. doi:10.1175/1520-0469(2003)060<0865:IAPCIM>2.0.CO;2
- Lyapustin, A. I. (2005). Radiative transfer code SHARM for atmospheric and terrestrial applications. *Appl. Opt.* 44, 7764. doi:10.1364/AO.44.007764
- Lyapustin, A., Wang, Y., Korkin, S., and Huang, D. (2018). MODIS collection 6 MAIAC algorithm. *Atmos. Meas. Tech.* 11, 5741–5765. doi:10.5194/amt-11-5741-2018
- Lyapustin, A., Wang, Y., Korkin, S., Kahn, R., and Winker, D. (2020). MAIAC thermal technique for smoke injection height from MODIS. *IEEE Geosci. Remote Sens. Lett.* 17, 730–734. doi:10.1109/LGRS.2019.2936332
- Lyapustin, A., Go, S., Korkin, S., Wang, Y., Torres, O., Jethva, H., et al. (2021a). Retrievals of aerosol optical depth and spectral absorption from DSCOVR EPIC. Front. Remote Sens. 2, 645794–14. doi:10.3389/frsen.2021.645794
- Lyapustin, A., Wang, Y., Go, S., Choi, M., Korkin, S., Huang, D., et al. (2021b). Atmospheric correction of DSCOVR EPIC: version 2 MAIAC algorithm. *Front. Remote Sens.* 2, 748362. doi:10.3389/frsen.2021.748362
- Lyapustin, A., Wang, Y., Korkin, S., Schaaf, C., Wang, W., and Wang, Z. (2025). Scaled RTLS BRDF model extended to high zenith angles. *Front. Remote Sens.* 6, 1533803. doi:10.3389/frsen.2025.1533803
- Maignan, F., Bréon, F. M., and Lacaze, R. (2004). Bidirectional reflectance of Earth targets: evaluation of analytical models using a large set of spaceborne measurements with emphasis on the hot spot. *Remote Sens. Environ.* 90, 210–220. doi:10.1016/j.rse. 2003.12.006
- Marquardt, D. W. (1963). An algorithm for least-squares estimation of nonlinear parameters. J. Soc. Ind. Appl. Math. 11, 431–441. doi:10.1137/0111030
- Marshak, A., Herman, J., Szabo, A., Blank, K., Carn, S., Cede, A., et al. (2018). Earth observations from DSCOVR epic instrument. *Bull. Am. Meteorol. Soc.* 99, 1829–1850. doi:10.1175/BAMS-D-17-0223.1
- Martins, J. V., Fernandez-Borda, R. A., Puthukkudy, A., Xu, X., Sienkiewicz, N., Smith, R., et al. (2024). "First results and on-orbit performance of the hyper-angular

- rainbow polarimeter (HARP2) on the PACE satellite," in *Sensors, systems, and next-generation satellites XXVIII.* Editors T. Kimura, S. R. Babu, and A. Hélière (SPIE), 10. doi:10.1117/12.3034008
- Moosmüller, H., and Chakrabarty, R. K. (2011). Technical note: simple analytical relationships between Ångström coefficients of aerosol extinction, scattering, absorption, and single scattering albedo. *Atmos. Chem. Phys.* 11, 10677–10680. doi:10.5194/acp-11-10677-2011
- Nanda, S., de Graaf, M., Veefkind, J. P., Sneep, M., ter Linden, M., Sun, J., et al. (2020). A first comparison of TROPOMI aerosol layer height (ALH) to CALIOP data. *Atmos. Meas. Tech.* 13, 3043–3059. doi:10.5194/amt-13-3043-2020
- Ross, J., and Marshak, A. (1989). The influence of leaf orientation and the specular component of leaf reflectance on the canopy bidirectional reflectance. *Remote Sens. Environ.* 27, 251–260. doi:10.1016/0034-4257(89)90086-2
- Sanders, A. F. J., and de Haan, J. F. (2013). Retrieval of aerosol parameters from the oxygen a band in the presence of chlorophyll fluorescence. *Atmos. Meas. Tech.* 6, 2725–2740. doi:10.5194/amt-6-2725-2013
- Schuster, G. L., Dubovik, O., and Arola, A. (2016). Remote sensing of soot carbon part 1: distinguishing different absorbing aerosol species. *Atmos. Chem. Phys.* 16, 1565–1585. doi:10.5194/acp-16-1565-2016
- Sinyuk, A., Holben, B. N., Eck, T. F., Giles, D. M., Slutsker, I., Korkin, S., et al. (2020). The AERONET version 3 aerosol retrieval algorithm, associated uncertainties and comparisons to version 2. *Atmos. Meas. Tech.* 13, 3375–3411. doi:10.5194/amt-13-3375-
- Sun, J., Veefkind, P., Nanda, S., van Velthoven, P., and Levelt, P. (2019). The role of aerosol layer height in quantifying aerosol absorption from ultraviolet satellite observations. *Atmos. Meas. Tech.* 12, 6319–6340. doi:10.5194/amt-12-6319-2019
- Thalman, R., and Volkamer, R. (2013). Temperature dependent absorption cross-sections of O2–O2 collision pairs between 340 and 630 nm and at atmospherically relevant pressure. *Phys. Chem. Chem. Phys.* 15, 15371. doi:10.1039/c3cp50968k
- Torres, O., Bhartia, P. K., Herman, J. R., Ahmad, Z., and Gleason, J. (1998). Derivation of aerosol properties from satellite measurements of backscattered ultraviolet radiation: theoretical basis. *J. Geophys. Res. Atmos.* 103, 17099–17110. doi:10.1029/98JD00900
- Torres, O., Ahn, C., and Chen, Z. (2013). Improvements to the OMI near-UV aerosol algorithm using A-train CALIOP and AIRS observations. *Atmos. Meas. Tech.* 6, 3257–3270. doi:10.5194/amt-6-3257-2013
- Torres, O., Jethva, H., Ahn, C., Jaross, G., and Loyola, D. G. (2020). TROPOMI aerosol products: evaluation and observations of synoptic-scale carbonaceous aerosol plumes during 2018-2020. *Atmos. Meas. Tech.* 13, 6789–6806. doi:10.5194/amt-13-6789-2020
- Val Martin, M., Logan, J. A., Kahn, R. A., Leung, F.-Y., Nelson, D. L., and Diner, D. J. (2010). Smoke injection heights from fires in North America: analysis of 5 years of satellite observations. *Atmos. Chem. Phys.* 10, 1491–1510. doi:10.5194/acp-10-1491-2010
- van der Werf, G. R., Randerson, J. T., Giglio, L., van Leeuwen, T. T., Chen, Y., Rogers, B. M., et al. (2017). Global fire emissions estimates during 1997–2016. *Earth Syst. Sci. Data* 9, 697–720. doi:10.5194/essd-9-697-2017
- Wanner, W., Li, X., and Strahler, A. H. (1995). On the derivation of kernels for kernel-driven models of bidirectional reflectance. *J. Geophys. Res. Atmos.* 100, 21077–21089. doi:10.1029/95JD02371
- Wei, J., Wang, J., Li, Z., Kondragunta, S., Anenberg, S., Wang, Y., et al. (2023). Long-term mortality burden trends attributed to black carbon and PM2·5 from wildfire emissions across the continental USA from 2000 to 2020: a deep learning modelling study. *Lancet Planet. heal.* 7, e963–e975. doi:10.1016/S2542-5196(23)00235-8
- Westerling, A. L., Hidalgo, H. G., Cayan, D. R., and Swetnam, T. W. (2006). Warming and earlier spring increase Western U.S. forest wildfire activity. *Sci. (80-)* 313, 940–943. doi:10.1126/science.1128834
- Xu, F., Dubovik, O., Zhai, P.-W., Diner, D. J., Kalashnikova, O. V., Seidel, F. C., et al. (2016). Joint retrieval of aerosol and water-leaving radiance from multispectral, multiangular and polarimetric measurements over ocean. *Atmos. Meas. Tech.* 9, 2877–2907. doi:10.5194/amt-9-2877-2016
- Xu, X., Wang, J., Wang, Y., Zeng, J., Torres, O., Reid, J. S., et al. (2019). Detecting layer height of smoke aerosols over vegetated land and water surfaces via oxygen absorption bands: hourly results from EPIC/DSCOVR in deep space. *Atmos. Meas. Tech.* 12, 3269–3288. doi:10.5194/amt-12-3269-2019
- Xu, F., van Harten, G., Diner, D. J., Kalashnikova, O. V., Seidel, F. C., Bruegge, C. J., et al. (2017). Coupled retrieval of aerosol properties and land surface reflection using the airborne multiangle SpectroPolarimetric imager. *J. Geophys. Res.* 122, 7004–7026. doi:10.1002/2017JD026776
- Xu, X., Wang, J., Wang, Y., Zeng, J., Torres, O., Yang, Y., et al. (2017). Passive remote sensing of altitude and optical depth of dust plumes using the oxygen A and B bands: first results from EPIC/DSCOVR at Lagrange-1 point. *Geophys. Res. Lett.* 44, 7544–7554. doi:10.1002/2017GL073939
- Zhou, Y., Zhai, P.-W., and Yang, Y. (2023). Evaluation of EPIC oxygen bands stability with radiative transfer simulations over the south pole. *J. Quant. Spectrosc. Radiat. Transf.* 310, 108737. doi:10.1016/j.jqsrt.2023.108737